Relation of short-range and long-range lithium ion dynamics in glass-ceramics: Insights from ^{7}Li NMR field-cycling and field-gradient studies

Michael Haaks,[1] Steve W. Martin,[2] and Michael Vogel[1,*]

[1]*Institut für Festkörperphysik, Technische Universität Darmstadt, Hochschulstr. 6, D-64289 Darmstadt, Germany*
[2]*Department of Materials Science and Engineering, Iowa State University, 2220E Hoover Hall, Ames, Iowa 50011, USA*

We use various ^{7}Li NMR methods to investigate lithium ion dynamics in 70Li$_2$S-30P$_2$S$_5$ glass and glass-ceramic obtained from this glass after heat treatment. We employ ^{7}Li spin-lattice relaxometry, including field-cycling measurements, and line-shape analysis to investigate short-range ion jumps as well as ^{7}Li field-gradient approaches to characterize long-range ion diffusion. The results show that ceramization substantially enhances the lithium ion mobility on all length scales. For the 70Li$_2$S-30P$_2$S$_5$ glass-ceramic, no evidence is found that bimodal dynamics result from different ion mobilities in glassy and crystalline regions of this sample. Rather, ^{7}Li field-cycling relaxometry shows that dynamic susceptibilities in broad frequency and temperature ranges can be described by thermally activated jumps governed by a Gaussian distribution of activation energies $g(E_a)$ with temperature-independent mean value $E_m = 0.43$ eV and standard deviation $\sigma = 0.07$ eV. Moreover, use of this distribution allows us to rationalize ^{7}Li line-shape results for the local ion jumps. In addition, this information about short-range ion dynamics further explains ^{7}Li field-gradient results for long-range ion diffusion. In particular, we quantitatively show that, consistent with our experimental results, the temperature dependence of the self-diffusion coefficient D is not described by the mean activation energy E_m of the local ion jumps, but by a significantly smaller apparent value whenever the distribution of correlation times $G(\log \tau)$ of the jump motion derives from an invariant distribution of activation energies and, hence, continuously broadens upon cooling. This effect occurs because the harmonic mean, which determines the results of diffusivity or also conductivity studies, continuously separates from the peak position of $G(\log \tau)$ when the width of this distribution increases.

I. INTRODUCTION

Rechargeable energy sources combining high safety, reliability, and energy density are of enormous significance as portable power supplies, e.g., for future electronic devices or electro mobility. All-solid-state lithium ion batteries are promising candidates in this application. Therefore, the development of such devices is one of the ultimate goals in materials research. Key to such endeavors is an availability of solid electrolyte materials showing enhanced transport of lithium ions. For a knowledge-based design of solid electrolytes with superior properties, detailed knowledge about the mechanisms of lithium ion conduction in various types of materials is required [1,2]. Although the technological relevance has triggered valuable progress in recent years, a detailed understanding of lithium ion dynamics in solids is, however, still lacking [3–7].

Ceramization, i.e., forming glass-ceramics and ceramics from glass, has proven particularly useful to produce solid electrolytes with ionic conductivities higher than 10^{-3} $(\Omega\,\text{cm})^{-1}$ at room temperature, rendering these materials interesting for use as solid electrolytes in lithium ion batteries [8]. In general, ceramization involves controlled crystallization and produces materials featuring both amorphous and crystalline phases. To this day, the origin of fast ion transport in ceramic materials is, however, not fully understood. In principle, the conductivity enhancement may be related to amorphous, crystalline, and/or interfacial regions in their heterogeneous

structures. To tackle this question, it is necessary to observe in which way microscopic ion jumps in diverse structural regions evolve into macroscopic charge transport and, hence, to study ion dynamics on various time and length scales.

^{7}Li NMR is a powerful tool for this purpose [9–12]. Combining various ^{7}Li NMR methods, it is possible to investigate lithium-ion jump motion in a broad time window, covering roughly ten orders of magnitude. In particular, ^{7}Li spin-lattice relaxation (SLR) analysis has a long-standing tradition in studies of local lithium-ion dynamics in solid electrolytes [13–16]. While traditional approaches used a single or, occasionally, a few magnetic fields B_0 and, thus, Larmor frequencies ω_L, recent studies showed that ^{7}Li field cycling (FC) enables measurements of the SLR time T_1 in a broad continuous range of ω_L values [17,18], providing straightforward access to the frequency-dependent spectral density of the lithium ion jump motion. In addition to these studies of lithium ion dynamics on local scales in homogeneous magnetic fields, ^{7}Li NMR experiments in magnetic field gradients allow one to observe lithium ion diffusion on mesoscopic scales on the order of 1 μm, in particular, to measure the self-diffusion coefficient D [11,13].

Appropriate ceramization turned out to be an advantageous strategy to improve the ionic conductivity of 70Li$_2$S-30P$_2$S$_5$ materials [8]. Specifically, it was shown that suitable heat treatment resulted in an increase of the conductivity at room temperature by more than an order of magnitude. Several studies addressed the origin of this improvement during the transformation from glass to glass-ceramic [8,19–23]. The enhanced conductivity was argued to result from a precipitation of high lithium ion conductivity metastable

---

*Corresponding author: michael.vogel@physik.tu-darmstadt.de

$Li_7P_3S_{11}$ crystal and to depend on the details of the heat treatment. Specifically, quantification of crystalline and amorphous fractions in various $70Li_2S$-$30P_2S_5$ glass-ceramics revealed higher conductivity for higher crystallinity [22]. Moreover, [7]Li field-gradient studies reported that the heterogeneous structure of the glass-ceramic, e.g., the existence of grain boundaries, leads to anomalous lithium ion diffusion with faster diffusion on short time and length scales than on longer scales [19,23].

Here, we exploit that ^{7}Li NMR methods yield detailed insights into lithium ion dynamics on various time and length scales to gain further insights into the mechanisms for lithium ion transport in $70Li_2S$-$30P_2S_5$ glass and, in particular, glass-ceramics. In detail, we perform [7]Li SLR measurements, including FC approaches, together with [7]Li line-shape (LS) analysis to ascertain microscopic ion dynamics. Furthermore, we use [7]Li field-gradient methods to investigate mesoscopic ion diffusion. While previous studies employed the pulsed field gradient (PFG) method, we utilize the static field gradient (SFG) technique, which allows us to apply stronger field gradients g and, thus, to extend the dynamic range of the experiment to smaller distances and slower diffusion. We show that [7]Li FC and LS studies enable straightforward determination of the broad distribution of activation energies for the lithium ion jumps. Moreover, we demonstrate that the Gaussian distribution $g(E_a)$ obtained from this analysis of the short-range ion dynamics allows us to rationalize our findings using [7]Li SFG diffusometry for the long-range ion transport via a rate average.

II. SAMPLE PREPARATION

A $70Li_2S$-$30P_2S_5$ amorphous sample was prepared by weighing appropriate amounts of Li_2S (Alfa-Aesar, 99%) and P_2S_5 (Sigma Aldrich, 99%) inside a N_2 glovebox. The N_2 glovebox had O_2 and H_2O levels of < 1 ppm. The powders were ground for 5 min in an agate mortar and pestle and then loaded into an 80-ml ZrO_2 pot. Twenty ZrO_2 balls, 10 mm in diameter, were used as the milling media. The sample to ball weight ratio was $\sim 1 : 20$. The pot was sealed under vacuum with a rubber gasket and taped shut to avoid air influx and contamination while the sample was being milled outside the glovebox. Samples were mechanically milled for 40 h using a high-energy planetary mono mill (Model Pulverisette 6, Fritsch) rotated at 370 rpm. The glass-ceramic powders were prepared by heat treating the amorphous powder at $280\,^\circ$C for 1 h. Infrared and Raman spectroscopies were used on the prepared amorphous samples to confirm complete chemical reaction between the Li_2S and P_2S_5 and that there were no detectable amounts of water or oxygen added to the samples during processing. X-ray diffraction and Raman spectroscopy were used to show the amorphous nature of the as-prepared powder and the crystalline structure of the heat treated glass-ceramic material.

III. THEORETICAL BACKGROUND

^{7}Li NMR studies of lithium ion jump motion exploit the fact that [7]Li spins are subject to diverse interactions in various environments so that, in general, they show different resonance frequencies when the corresponding lithium ions occupy distinguishable lithium sites. As a consequence, lithium ion jumps between various lithium sites render the resonance frequencies time dependent. [7]Li FC and LS studies are capable of probing this time dependence and, thus, the underlying site exchange rates of the lithium ions.

For [7]Li ($I = 3/2$), the Zeeman interaction as well as the quadrupolar and dipolar interactions determine the resonance frequencies. The Zeeman interaction leads to the Zeeman splitting, where the energy difference between the levels is determined by the Larmor frequency $\omega_L = \gamma B_0$, with the gyromagnetic ratio γ. The quadrupolar interaction, which results from the coupling of the nuclear quadrupole moment to an electric field gradient at the nuclear site, and the dipolar interaction, which describes the couplings of the nuclear magnetic moments, cause a shift of the Zeeman levels. In sufficiently high magnetic fields B_0, the Zeeman interaction of [7]Li is much stronger than its quadrupolar interaction, which, in turn, exceeds its dipolar interaction. In first order, the quadrupolar interaction affects the resonance frequencies of the satellite transitions $|\pm\frac{3}{2}\rangle \leftrightarrow |\pm\frac{1}{2}\rangle$, but not that of the central transition $|+\frac{1}{2}\rangle \leftrightarrow |-\frac{1}{2}\rangle$. Therefore, in the absence of motion, the ^{7}Li NMR spectra of disordered materials consist of a broad line, which is associated with the satellite transitions and reflects the distributed quadrupolar frequencies ω_Q in diverse local environments, and a narrow line, which is linked to the central transition and mirrors the weaker dipolar couplings. Usually, in this static limit, both lines are well described by Gaussian line shapes.

IV. EXPERIMENTAL DETAILS

[7]Li FC experiments were performed on a home-built relaxometer [24] with the magnetic field B_0 during the relaxation period varying between 12 μT and 1.5 T, corresponding to [7]Li Larmor frequencies in a range of 20 kHz to 12 MHz. The temperature was controlled by a flow of tempered nitrogen gas. Further experimental details can be found in previous works [17,18].

Additional [7]Li T_1 measurements were carried out on three home-built spectrometers operating at fixed B_0 fields of 4.7, 7.0, and 8.5 T, corresponding to $\omega_L = 2\pi \times 76$ MHz, $2\pi \times 118$ MHz, and $2\pi \times 140$ MHz, respectively. For these T_1 measurements, the saturation-recovery sequence was combined with solid-echo detection, 90°_x-Δ-64°_y-Δ-acquisition, where the echo delay was $\Delta = 20$ μs. ^{7}Li NMR spectra were recorded with the same pulse sequence at 4.7 T. In all setups and experiments, the 90° pulse length amounted to 2–3 μs, ensuring proper excitation of the broad static-limit spectra. The temperature was controlled by a liquid-nitrogen cryostat for the 4.7 and 7.0 T setups and by a nitrogen gas flow for the 8.5 T spectrometer.

To measure self-diffusion coefficients D, we utilized a home-built SFG diffusometer working at a magnetic field of 3.8 T ($\omega_L = 2\pi \times 63$ MHz) and a field gradient of $g = 72.8$ T/m, which is produced by a specially designed superconducting magnet with an antisymmetric arrangement of two field coils [25]. The stimulated echo sequence 90°_x-t_p-90°_y-t_m-90°_y-t_p was used to observe slow lithium ionic diffusion. To determine the self-diffusion coefficient D, we

varied the mixing time t_m for several fixed evolution times t_p (see below).

V. RESULTS

In the following, we apply ^{7}Li NMR methods to ascertain lithium ion dynamics in 70Li$_2$S-30P$_2$S$_5$ glass (LiPS-GL) and in a 70Li$_2$S-30P$_2$S$_5$ glass-ceramic (LiPS-GC), as obtained from this glass by heat treatment at 553 K for 1 h.

A. ^{7}Li NMR spin-lattice relaxation

First, we exploit that ^{7}Li SLR, i.e., the buildup of ^{7}Li equilibrium magnetization in the B_0 field, is usually determined by fluctuations of the ^{7}Li quadrupolar interaction produced by lithium ion dynamics. Specifically, for isotropic samples, the ^{7}Li SLR rate depends on the spectral density $J(\omega)$ of the fluctuations and, hence, of the lithium ion motion according to [9]

$$\frac{1}{T_1}(\omega_L) \propto J(\omega_L) + 4J(2\omega_L). \tag{1}$$

To exploit this relation, we analyze both the temperature and the frequency dependence of $1/T_1$. In the former approach, we expect a maximum of $1/T_1(T)$ when the lithium ion jump rates are on the order of the Larmor frequency, strictly speaking, when the associated fluctuations of the quadrupolar interaction are characterized by a correlation time $\tau \approx 1/\omega_L$ [9]. In the latter approach, $1/T_1(\omega_L)$ provides straightforward access to the frequency-dependent spectral density $J(\omega_L)$ [17,18]. We note in passing that the assumption of isotropic dynamics is not perfectly, but still approximately correct, as will become clear in the subsequent line-shape analysis from the observation of a dominant Lorentzian line at high temperatures. While we find a monoexponential buildup of the magnetization in all ^{7}Li SLR studies on LiPS-GC, we observe a two-step buildup for LiPS-GL in the high-field measurements. Such bimodality is unusual for glasses. Therefore, the structural integrity of the sample was confirmed by x-ray diffraction and Raman spectroscopy. In the following, we focus on the faster SLR process of LiPS-GL, which is still slower than that of LiPS-GC.

Figure 1 shows temperature-dependent SLR rates $1/T_1$ for LiPS-GC and LiPS-GL at exemplary Larmor frequencies ω_L. For LiPS-GC, $1/T_1$ maxima indicate lithium ion dynamics on the time scale $1/\omega_L$ in the studied temperature range. The maxima are located at higher temperatures for higher Larmor frequencies, reflecting the speedup of the motion upon heating. Furthermore, the maxima are higher at lower Larmor frequencies, consistent with the general expectation from SLR theory [9,13]. By contrast, $1/T_1$ maxima are not observed for LiPS-GL. Rather, the SLR rate monotonically decreases upon cooling, implying that lithium ion dynamics is slow on the time scale $1/\omega_L$ in the whole accessible temperature range below the glass transition. Taken together these findings reveal that local lithium ion dynamics is faster in LiPS-GC than in LiPS-GL.

For LiPS-GC, it is possible to obtain temperature-dependent correlation times τ from the observed shift of the $1/T_1$ maxima when the Larmor frequency is varied in the broad range accessible in the present approach. For simple ion dynamics
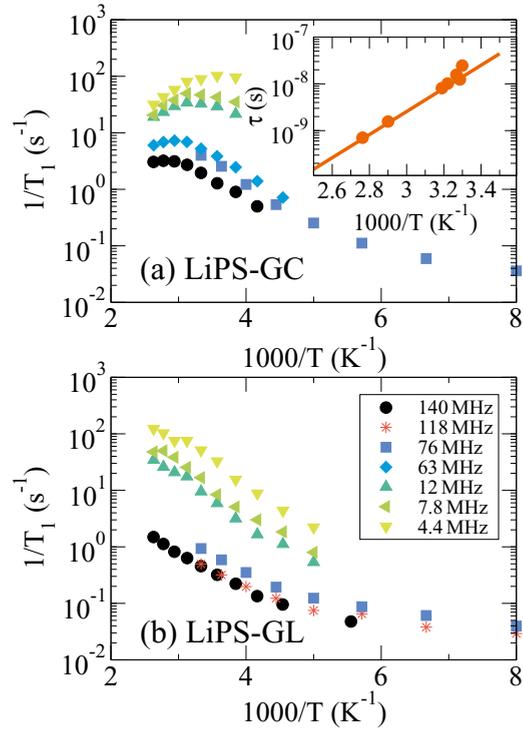
FIG. 1. ^{7}Li SLR rate $1/T_1$ as a function of inverse temperature for (a) LiPS-GC and (b) LiPS-GL at several Larmor frequencies. The indicated values $\omega_L/(2\pi)$ apply to both samples. The inset in panel (a) shows correlation times τ of lithium ion dynamics in LiPS-GC, as obtained at different Larmor frequencies from $\tau(T_{max}) = 0.616\,\omega_L^{-1}$ where T_{max} denotes the temperature of the respective $1/T_1$ maximum. The straight line is an Arrhenius fit, yielding an activation energy of $E_a = 0.49$ eV.

characterized by a single exponential correlation function and a Lorentzian spectral density, $J(\omega_L) = \tau/(1 + \omega_L^2\tau^2)$, the relation $\tau(T_{max}) = 0.616\,\omega_L^{-1}$ applies, where T_{max} is the temperature at which the $1/T_1$ maximum is located. The temperature-dependent correlation times resulting from this relation are shown in the inset of Fig. 1(a). We see that the results are well described by an Arrhenius law with an activation energy of $E_a = 0.49$ eV, which is larger than $E_a = 0.33$ eV from dc conductivity measurements [19]. We will rationalize this apparent discrepancy below when discussing the diffusion experiments. Strictly speaking, a Lorentzian spectral density does not describe the complex ion dynamics in the studied disordered samples, where a distribution rather than a single correlation time may be expected. Then, the relation $\tau(T_{max}) = 0.616\,\omega_L^{-1}$ is not necessarily valid. While this relation breaks down for asymmetric distributions $G(\log \tau)$, it still applies to symmetric ones, in particular, to our case of logarithmic Gaussian distributions $G(\log \tau)$ (see below). In the latter case, the analysis yields the peak position of $G(\log \tau)$, i.e., the mean value on a logarithmic scale.

Next, we use ^{7}Li FC relaxometry to obtain straightforward insights into the frequency dependence of the SLR rate. Motivated by previous FC work [26], including our ^{7}Li FC studies [17,18], we exploit the fluctuation-dissipation relation between the imaginary parts of dynamic susceptibilities and the spectral densities, $\chi''(\omega) = \omega J(\omega)$, and present the
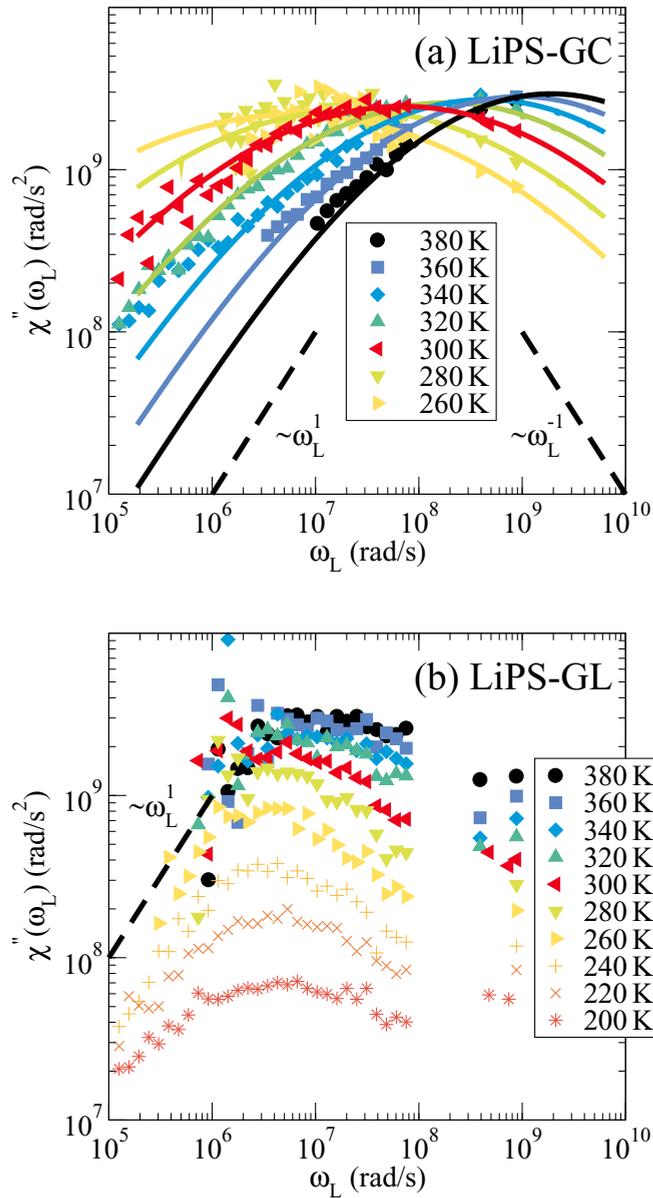
FIG. 2. NMR susceptibility $\chi''(\omega_L) = \omega_L/T_1(\omega_L)$ for (a) LiPS-GC and (b) LiPS-GL at various temperatures. In panel (a), the solid lines are fits using a Gaussian distribution of activation energies $g(E_a)$ with a mean value $E_m = 0.43$ eV and a standard deviation $\sigma = 0.07$ eV together with an Arrhenius prefactor $\tau_0 = 5.2 \times 10^{-16}$ s (see text for details). The asymptotic behaviors of a Debye peak, $\omega_L^{\pm 1}$, are indicated by dashed lines.

results in the form of a generalized "NMR susceptibility" defined as $\chi''(\omega_L) = \omega_L/T_1(\omega_L)$. This representation enables an interpretation in analogy with results from electrical and/or mechanical relaxation studies. In particular, the time scale of the dynamics is readily available from the peak position of $\chi''(\omega_L)$.

In Fig. 2, we present $\chi''(\omega_L)$ for the studied samples. For LiPS-GC, we see a broad susceptibility maximum, which shifts to lower frequencies upon cooling, reflecting the slowdown of the lithium ion motion. In addition, it is evident that the susceptibility maximum has an essentially temperature-

independent height, indicating that the mechanism for ^{7}Li SLR and the strength of the relevant quadrupolar interaction are basically unchanged in the studied temperature range. If lithium ion dynamics were described by a single exponential correlation function, a Debye peak would result for $\chi''(\omega_L)$ with slopes ω_L^{+1} and ω_L^{-1} on the low- and high-frequency flanks, respectively. Clearly, $\chi''(\omega_L)$ is significantly broadened with respect to the Debye case. Hence, the correlation functions of lithium ion dynamics in LiPS-GC are strongly nonexponential.

To model the broadening of $\chi''(\omega_L)$, we assume that the lithium ions perform thermally activated jumps governed by a temperature-independent Gaussian distribution of activation energies

$$g(E_a) = \frac{1}{\sqrt{2\pi}\sigma} \exp\left(-\frac{(E_a - E_m)^2}{2\sigma^2}\right) \quad (2)$$

and use the Arrhenius law

$$\tau = \tau_0 \exp\left(\frac{E_a}{k_B T}\right) \quad (3)$$

to map the distributed activation energies E_a onto the corresponding correlation times τ at a given temperature, yielding $G(\log \tau)$. The temperature-dependent distribution of correlation times, in turn, allows us to calculate the NMR susceptibility according to

$$\chi''(\omega_L) = \int_{-\infty}^{+\infty} [\chi_D''(\omega_L\tau) + 4\chi_D''(2\omega_L\tau)]G(\log \tau)d\,\log\tau,$$

$$(4)$$

where the imaginary part of the Debye susceptibility is given by $\chi_D''(\omega\tau) = \omega\tau/(1 + \omega^2\tau^2)$. In Fig. 2, we see that fitting this model to the measured NMR susceptibilities accurately describes $\chi''(\omega_L)$ in broad frequency and temperature ranges. The temperature-independent Gaussian distribution of activation energies $g(E_a)$ resulting from these fits is characterized by a mean energy $E_m = 0.43$ eV and a standard deviation $\sigma = 0.07$ eV. The former value is in reasonable agreement with the above result of the temperature-dependent analysis, further described below. The latter value reveals that the lithium ion jump motion in LiPS-GC is subject to pronounced dynamic heterogeneity, in particular, at low temperatures where very broad distributions of correlation times result as a consequence of the fact that the width of $G(\log \tau)$ increases with $1/T$ for thermally activated jumps governed by a temperature-independent distribution $g(E_a)$.

For LiPS-GL, $\chi''(\omega_L)$ shows a different behavior. We do not observe a clear susceptibility maximum, which shifts through the frequency window when the temperature is varied; rather, $\chi''(\omega_L)$, at $\omega_L \geqslant 10^6$ rad/s, weakly decreases with increasing frequency and the value at a given frequency strongly grows with increasing temperature. These findings suggest that the ^{7}Li SLR of LiPS-GL is not governed by a site exchange of lithium ions in the studied frequency and temperature ranges, consistent with the absence of $1/T_1$ maxima for this sample, but other contributions to ^{7}Li SLR may dominate, e.g., contributions from two-level systems [27] or impurities [28,29]. At frequencies $\omega_L < 10^6$ rad/s and low temperatures, ^{7}Li $1/T_1$ data should not be interpreted in terms of lithium ion motion at all [18]. At such low frequencies and, hence, low

magnetic fields, the Zeeman interaction is weak. Moreover, at sufficiently low temperatures, the quadrupolar interaction is not averaged by lithium ion motion. Taken together, this means that the Zeeman interaction no longer dominates the quadrupolar interaction and, hence, the usual perturbation approach to SLR breaks down. The following ^{7}Li LS analysis reveals that lithium ion motion is too slow to fully average the quadrupolar interaction below 300 K for the studied samples. Therefore, ^{7}Li $1/T_1$ data at $\omega_L < 10^6$ rad/s and $T < 300$ K should be discarded. Nevertheless, to demonstrate the effect, such data are included for LiPS-GL.

B. ^{7}Li NMR spectra

In the low-temperature (LT) limit, where lithium ion dynamics are negligible, the ^{7}Li NMR spectra of disordered samples are comprised of broad Gaussian and narrow Gaussian peaks. These components are related to the satellite and central transitions of the ^{7}Li nuclei and reflect the diversity of their quadrupolar and dipolar interactions in various environments (see Sec. III). Upon increasing the temperature, the ^{7}Li NMR spectra undergo a characteristic motional narrowing when the time scale of the lithium ion jumps crosses the time scale of the experiment, which is given by the inverse spectral width in static situations, $1/\Delta\omega$. In the high-temperature (HT) limit, where the lithium ions show rapid site exchange, the ^{7}Li NMR spectra reflect the motionally averaged quadrupolar and dipolar interactions. The shape of these spectra provides information about the geometry of the lithium ion motion. While fast isotropic motion results in complete averaging of these interactions and, hence, in narrow Lorentzians, fast anisotropic motion leads to incomplete averaging and, as a consequence, to non-Lorentzian spectra of some residual width. Hence, ^{7}Li LS analysis provides valuable insights into both rate and geometry of lithium ion dynamics.

In Figs. 3 and 4, we show the temperature-dependent ^{7}Li NMR spectra of LiPS-GL and LiPS-GC, respectively. While the LT spectra are comparable for both samples, the motional-narrowing schemes are different. For LiPS-GL, the Gaussian spectra evolve into Lorentzian lines when lithium ion dynamics becomes faster upon heating. Thus, the HT spectra are indicative of isotropic motion, consistent with the overall isotropy of glasses. For LiPS-GC, the LS collapse does not result in a Lorentzian line. Rather, the HT spectra consist of a narrow line and a broader foot, which has neither Gaussian nor Lorentzian shape and a temperature-independent width of ~15 kHz over a broad temperature range. These findings imply that a fraction of the lithium ions in LiPS-GC, presumably ions in the crystalline phase of the glass-ceramic, show anisotropic motion. In addition, comparison of the ^{7}Li NMR spectra at intermediate temperatures, e.g., at 200 K, reveals that motional narrowing is more advanced in LiPS-GC than in LiPS-GL and, hence, lithium ion dynamics is faster in the former than in the latter sample, consistent with our relaxometry results.

For quantitative ^{7}Li LS analysis, it is necessary to consider that lithium ion dynamics in LiPS-GC (see Fig. 2) and, most probably, also in LiPS-GL is characterized by a very broad distribution of correlation times, $G(\log \tau)$. Under such circumstances, slow ($\tau \gg 1/\Delta\omega$) and fast ($\tau \ll 1/\Delta\omega$) lithium ions coexist at suitable temperatures, while contributions from the
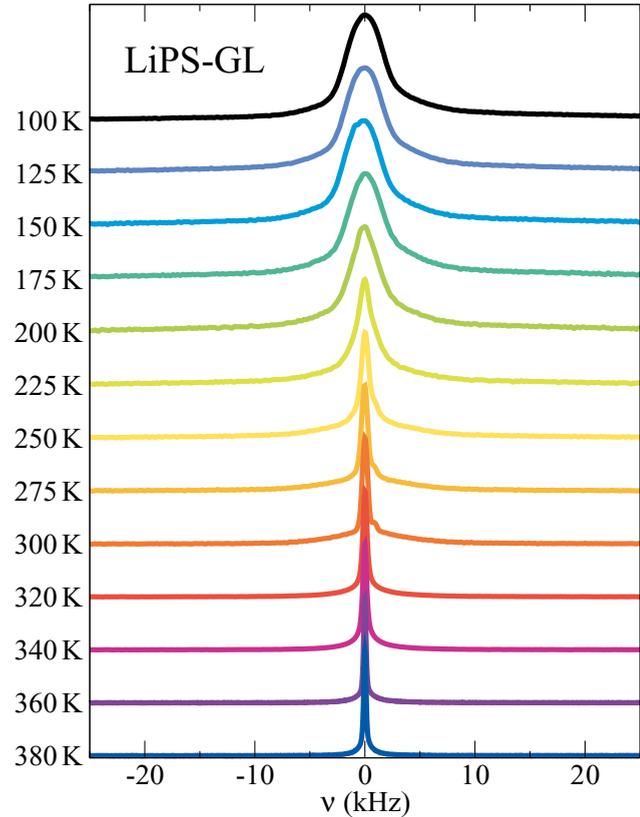
FIG. 3. Temperature-dependent ^{7}Li NMR spectra of LiPS-GL.

fraction in the intermediate motional regime are negligible. Then, it is possible to describe the temperature-dependent ^{7}Li NMR spectra $S(\omega, T)$ by a weighted superposition of the normalized temperature-independent LT and HT spectra, $S_{LT}(\omega)$ and $S_{HT}(\omega)$ [9,17,30–32]:

$$S(\omega, T) = W(T)S_{HT}(\omega) + [1 - W(T)]S_{LT}(\omega), \quad (5)$$

where the weighting factor is given by

$$W(T) = \int_{-\infty}^{\log(1/\Delta\omega)} G(\log \tau) d \log \tau. \quad (6)$$

Closer inspection of Figs. 3 and 4 confirms that such two-component lines exist at intermediate temperatures. In the following, we will exploit that, for LiPS-GC, $G(\log \tau)$ is known from the above ^{7}Li FC relaxometry study.

For LiPS-GC, we find that such weighted superposition of the LT and HT limits well describes the ^{7}Li NMR spectra at all studied temperatures. Figure 5 shows the weighting factor $W(T)$ obtained from these LS fits. We see that the LS transition takes place in a relatively broad temperature range between 150 and 250 K. To rationalize this finding, we exploit that knowledge of the distribution of correlation times allows us to calculate the weighting factor. Specifically, we obtain $G(\log \tau)$ at the relevant temperatures from the above determined distribution of activation energies, $g(E_a)$, and calculate $W(T)$ based on Eq. (6) using $\Delta\omega = 2\pi \times 20.2$ kHz, as obtained from the spectra below 150 K. In Fig. 5, it can be seen that the experimental and calculated weighting factors $W(T)$ are in good agreement. Thus, ^{7}Li SLR and LS
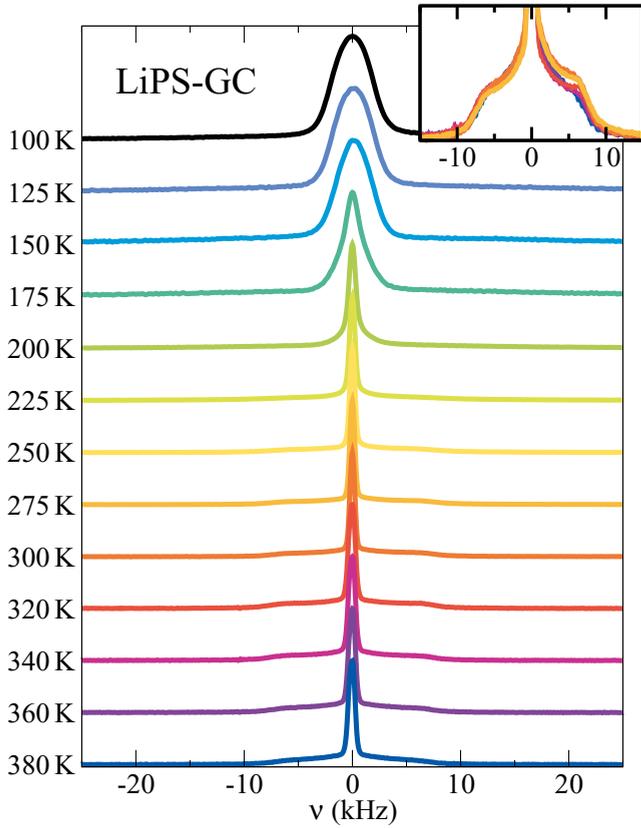
FIG. 4. Temperature-dependent ^{7}Li NMR spectra of LiPS-GC. The inset shows the central region of the spectra at temperatures 275–380 K in more detail. The color code is the same as in the main panel.

FIG. 5. Results from ^{7}Li LS analysis for LiPS-GC and LiPS-GL using Eqs. (5) and (6). The weighting factor $W(T)$ describes the contribution of the motionally narrowed line to the total spectral intensity. For LiPS-GC, the experimental results are compared with weighting factors (solid line) calculated based on the Gaussian distribution of activation energies $g(E_a)$ from our SLR studies (see text for details).

analyses yield fully consistent information about local lithium ion dynamics in LiPS-GC.

For LiPS-GL, the ^{7}Li NMR spectra at intermediate temperatures are poorly described by a simple superposition of the LT and HT spectra. Therefore, we drop the assumption that these LS components have temperature-independent shapes. Specifically, we fit the ^{7}Li NMR by a superposition of two Gaussians, which reflect the LT components, and a Lorentzian, which represents the HT component, allowing for temperature-dependent width parameters of these lines. This approach enables good interpolation of the experimental data. The resulting weighting factors $W(T)$ are included in Fig. 5. We observe that the LS transition of LiPS-GL occurs at higher temperatures and in a broader range, as compared to LiPS-GC. The former finding confirms that ceramization speeds up local lithium ion dynamics. The latter result implies that $G(\log \tau)$ is even broader for LiPS-GL than for LiPS-GC so that a broader temperature interval is required to fully shift this distribution over the experimental time scale $1/\Delta\omega$. We note in passing that measurements of ^{7}Li NMR spectra with various relaxation delays did not yield evidence that the Gaussian and Lorentzian spectral components of LiPS-GL are related to the bimodal buildup of the magnetization for this sample.

C. Diffusion measurements

After characterization of lithium ion dynamics on local scales by means of ^{7}Li SLR and LS analyses, we continue with

measurements of lithium ion diffusion on micrometer scale using ^{7}Li SFG approaches. The latter method exploits that, in gradient fields, the nuclear positions determine the Larmor frequencies and, as a consequence, lithium ion diffusion manifests itself in a time dependence $\omega_L(t)$. Here, we use the stimulated-echo sequence (see Sec. IV) to correlate the resonance frequencies at two times and, thus, to probe this time dependence. Specifically, we observe the height of the stimulated echo as a function of the mixing time t_m for fixed evolution time t_p to determine the self-diffusion coefficient D. For free diffusion, the stimulated-echo decay depends on the self-diffusion coefficient D according to

$$S(t_m; t_p) \propto \exp\left[-\gamma^2 g^2 t_p^2 D\left(\tfrac{2}{3}t_p + t_m\right)\right]. \quad (7)$$

The length scale of the SFG experiment depends on the factor $(\gamma g t_p)^{-1}$ and amounts to $\sim 1\,\mu m$ in our case.

In Fig. 6, we present results from ^{7}Li SFG diffusometry on LiPS-GC at 360 K. We see that, when the evolution time t_p is extended, the stimulated-echo amplitude is reduced and the stimulated-echo decay shifts to shorter mixing times t_m. The reduction of the amplitude is a mere consequence of the action of spin-spin relaxation during the evolution times. The shift of the decays is expected due to the evolution-time dependent length scale of the experiment; in particular, the time constant of the decays scales as t_p^{-2} for free diffusion [see Eq. (7)]. For a quantitative analysis, we simultaneously fit the stimulated-echo decays for all values of t_p to Eq. (7). In Fig. 6, inspection of the fit results reveals that a single self-diffusion coefficient D describes all data sets, indicating that lithium ion motion in LiPS-GC on a micrometer scale is well described by the model of free diffusion. Thus, the findings of our SFG study do not confirm the outcome of previous PFG work [19], which reported anomalous diffusion with a length-scale-dependent diffusivity.

Figure 7 shows the self-diffusion coefficients D obtained for LiPS-GC and LiPS-GL from analogous analyses in broad
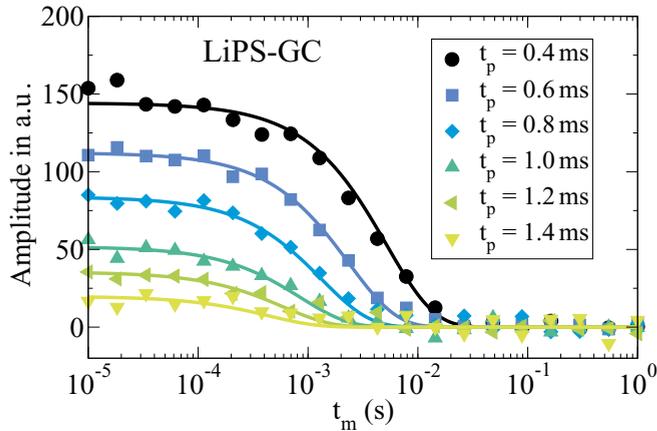
FIG. 6. Results from ^{7}Li SFG diffusometry on LiPS-GC at 360 K. Stimulated-echo decays for various evolution times t_p are compared. Global fits to Eq. (7) are shown as solid lines. In these fits, the stimulated-echo decays for all evolution times are interpolated using the *same* diffusion coefficient D.

FIG. 8. Experimental correlation times of LiPS-GC obtained from the position of the $1/T_1$ maxima (τ_{T1}) and from the self-diffusion coefficients D according to $\tau_D = a^2/(6D)$ with $a = 0.52$ Å. For comparison, the correlation times τ_m and τ_r are included, which were calculated from the distribution of activation energies $g(E_a)$ obtained from ^{7}Li FC relaxometry. While τ_m denotes the peak position of the corresponding distribution of correlation times $G(\log \tau)$, τ_r is the harmonic mean of this distribution, i.e., a rate average.

temperature ranges. It is evident that lithium ion diffusion is about an order of magnitude faster in LiPS-GC than in LiPS-GL. The temperature dependence of the lithium ion diffusivities can be roughly described by Arrhenius laws with activation energies of $E_a = 0.28$ eV for LiPS-GC and $E_a = 0.26$ eV for LiPS-GL. Hence, there are only minor differences of the activation energies. For comparison, Fig. 7 displays D values previously calculated from the dc conductivity based on the Nernst-Einstein relation [19]. We find that the results of diffusion and conduction studies are in reasonable agreement. Both approaches reveal that the room-temperature lithium ion mobility can be enhanced by about an order of magnitude upon ceramization. On the other hand, for LiPS-GC, the activation energy $E_a = 0.28$ eV from our diffusometry study

is significantly smaller than $E_m = 0.43$ eV from the above relaxometry approach.

D. Relation between lithium ion dynamics on different length scales

In the following, we determine the relation between lithium ion migration and local jump dynamics in more detail. For the simple case of a random walk with elementary jumps characterized by a single correlation time τ and a single step size a, diffusion coefficient and correlation time are related according to

$$D = \frac{a^2}{6\tau}. \tag{8}$$

In our case, the local jump dynamics are, however, as described above, characterized by logarithmic Gaussian distributions $G(\log \tau)$. Under such circumstances, it is necessary to consider that different experiments probe different averages over the distribution of correlation times. ^{7}Li NMR relaxometry yields the correlation time τ_m, which marks the position of the peak of $G(\log \tau)$ and, hence, corresponds to a logarithmic average. By contrast, ^{7}Li NMR diffusometry provides diffusivities, which in general reflect rate averages over distributed dynamics [33]. Therefore, a corresponding mean correlation time can be defined as the harmonic mean $\tau_r = \langle 1/\tau \rangle^{-1}$, where the pointed brackets denote the average over the distribution $G(\log \tau)$.

To calculate the relevant mean correlation times for LiPS-GC, we exploit that the temperature-independent distribution $g(E_a)$ from ^{7}Li FC yields $G(\log \tau)$ at all temperatures via the Arrhenius law. Figure 8 shows the so obtained temperature dependence of τ_m and τ_r. We see that τ_m is about two orders of magnitude longer than τ_r near room temperature, reflecting the well-known fact that the rate average and, thus, the diffusion experiment, are dominated by the fast ions of a distribution. More interestingly, the temperature dependence is significantly

FIG. 7. Temperature-dependent self-diffusion coefficients D of LiPS-GC and LiPS-GL from ^{7}Li SFG experiments. The solid lines are fits with an Arrhenius law, yielding activation energies of $E_a = 0.28 \pm 0.02$ eV and $E_a = 0.26 \pm 0.02$ eV, respectively. The dotted lines are diffusion coefficients previously calculated from the dc conductivity using the Nernst-Einstein relation [19].

higher for τ_m than for τ_r. It is trivial that τ_m follows an Arrhenius law characterized by the mean activation energy E_m. By contrast, the temperature dependence of τ_r is determined not only by the shift of $G(\log \tau)$, but also by the broadening of this distribution upon cooling.

For thermally activated jumps governed by an invariant distribution of activation energies, $G(\log \tau)$ broadens with $1/T$ when the temperature is decreased so that the fast correlation times of this distribution, which determine the rate average, increasingly differ from the most probable ones. Explicitly, for a Gaussian distribution $g(E_a)$ with width parameter σ_E, the logarithmic Gaussian distribution $G(\log \tau)$ has a temperature-dependent width parameter $\sigma_{\log \tau}(T) = \sigma_E/(k_B T \ln 10)$, leading to [33]

$$\frac{\tau_r}{\tau_m}(T) = \exp\left(-\frac{[\ln 10 \, \sigma_{\log \tau}(T)]^2}{2}\right) = \exp\left(-\frac{\sigma_E^2}{2k_B^2 T^2}\right),$$
(9)

which is known as Bässler's law [34]. As a consequence, τ_r does not obey an Arrhenius law. Rather, the temperature dependence of this mean value is described by an apparent activation energy

$$E_{app}(T) = E_m - \frac{\sigma_E^2}{2k_B T}.$$
(10)

In Fig. 8, it can be seen for LiPS-GC that the broadening of $G(\log \tau)$ upon cooling results in, first, a significantly weaker temperature dependence of τ_r as compared to τ_m and, second, a notable downward bending of $\log \tau_r(1/T)$.

These considerations put us into the position to investigate whether the diverse behaviors of various mean correlation times allow us to explain the different temperature dependence observed in our [7]Li SLR and SFG studies. In Fig. 8, it is evident that the values of τ_m are in good agreement with the correlation times obtained from the positions of the $1/T_1$ maxima [see Fig. 1(a)], confirming that our frequency-dependent and temperature-dependent SLR studies yield consistent results. For a discussion of the SFG results, we use Eq. (8) to calculate a "diffusion correlation time" $\tau_D = a^2/(6D)$ from the experimental self-diffusion coefficients. In doing so, the best overlap with τ_r is obtained for the jump length of $a = 0.52$ Å, which is somewhat smaller than the typical next neighbor distances of the lithium ions in solid electrolytes. We find that τ_D and τ_r agree well in the whole studied temperature range. Hence, the temperature dependence of the long-range ion diffusion can be fully explained by the distribution of activation energies $g(E_a)$ of the short-range ion jumps. In particular, the reduced temperature dependence of the self-diffusion coefficient D is a mere consequence of the fact that this quantity is determined by a rate average over the distributed dynamics, which depends not only on the shift, but also on the width of the distribution. Hence, when comparing results from different experimental techniques, including conductivity studies, it is mandatory to consider the respective effect of the temperature-dependent broadening of $G(\log \tau)$ on the quantities under study.

VI. SUMMARY AND CONCLUSION

We used various ^{7}Li NMR methods to characterize lithium ion dynamics in LiPS-GC and LiPS-GL. The results consistently show that ceramization enhances the lithium ionic mobility on all length scales. [7]Li SFG studies showed that the self-diffusion coefficient D on a micrometer scale is about an order of magnitude higher in LiPS-GC than in LiPS-GL at ambient temperatures, consistent with dc conductivity data, while the present measurements do not yield evidence for a significantly different temperature dependence of the diffusivity in these samples. Moreover, [7]Li SLR and LS analyses indicated that the lithium ion jump motions on a local scale become faster upon ceramization. Specifically, defined [7]Li $1/T_1$ maxima were observed for LiPS-GC, while this feature, indicative of lithium ionic motion on a time scale $1/\omega_L$, is expected to occur only above the accessible temperature range for LiPS-GL. Likewise, the motional narrowing regime of [7]Li spectra occurs at lower temperatures for the GC than for the GL sample.

For LiPS-GC, none of the ^{7}Li NMR approaches yielded evidence for bimodal lithium ion dynamics. For example, SLR and SFG data obeyed monoexponential behavior. Thus, a simple picture that the lithium ion mobility is high in the crystalline regions of this sample and slow in the glassy ones does not apply. Rather, [7]Li FC experiments revealed a broad, but continuous distribution of activation energies for the lithium ion jumps in LiPS-GC. Specifically, it was possible to describe NMR susceptibilities $\chi''(\omega_L)$ in broad frequency and temperature ranges by a temperature-independent Gaussian distribution $g(E_a)$, which is characterized by a mean energy $E_m = 0.43$ eV and a standard deviation $\sigma = 0.07$ eV. Use of this distribution also allowed us to quantitatively rationalize [7]Li two-component spectra in a broad temperature range of motional narrowing, indicating that [7]Li FC and LS studies yield a fully consistent picture of lithium ion jump motion in LiPS-GC. In the case of LiPS-GL, lithium ion dynamics was too slow to determine the distribution $g(E_a)$ by means of [7]Li FC in the accessible temperature range below the glass transition.

Finally, we investigated the relation between the short-range and long-range lithium ion dynamics in LiPS-GC. It was shown that our findings for the elementary jumps are fully consistent with that for the ion diffusion. The key to a common understanding of results from different experimental techniques is the notion that different observables reflect different averages of the broadly distributed dynamics. While NMR studies of local dynamics are dominated by the most probable correlation times of the distribution $G(\log \tau)$, NMR studies of diffusive motion probe a rate average and, hence, they are governed by the fast part of the distribution. This difference is of particular importance when the lithium ion motion can be derived from a temperature-independent distribution of activation energies $g(E_a)$ so that the resulting distribution of correlation times $G(\log \tau)$ not only shifts but also broadens upon cooling. In this way, the temperature dependence of the self-diffusion coefficient D does not reflect the mean activation energy, but it is reduced because of the fact that the harmonic mean continuously separates from the peak position when the width of $G(\log \tau)$ increases. This

effect allowed us to quantitatively explain that ^{7}Li NMR studies of short-range jumps and long-range diffusion yield different activation energies of 0.43 and 0.28 eV, respectively. We emphasize that the relevance of these effects is not at all restricted to NMR studies, but the fact that, for broadening distributions $G(\log \tau)$, the harmonic mean and the peak position show a different temperature dependence also needs to be considered for other observables, e.g., when comparing

results from electrical conductivity and mechanical relaxation studies.

[1] M. Park, X. Zhang, M. Chung, G. B. Less, and A. M. Sastry, J. Power Sources **195**, 7904 (2010).

[2] S. W. Martin, in *Handbook of Solid State Batteries*, edited by N. Dudney, W. West, and J. Nanda (World Scientific, Singapore, 2015), Vol. 6, pp. 433–501.

[3] J. C. Dyre and T. B. Schrøder, Rev. Mod. Phys. **72**, 873 (2000).

[4] A. Bunde, K. Funke, and M. D. Ingram, Solid State Ionics **86**, 1311 (1996).

[5] P. Maass, M. Meyer, A. Bunde, and W. Dieterich, Phys. Rev. Lett. **77**, 1528 (1996).

[6] J. B. Goodenough, Proc. R. Soc. A **393**, 215 (1984).

[7] J. C. Dyre, P. Maass, B. Roling, and D. L. Sidebottom, Rep. Prog. Phys. **72**, 046501 (2009).

[8] F. Mizuno, A. Hayashi, K. Tadanaga, and M. Tatsumisago, Adv. Mater. **17**, 918 (2005).

[9] R. Böhmer, K. Jeffrey, and M. Vogel, Prog. Nucl. Magn. Reson. Spectrosc. **50**, 87 (2007).

[10] C. Brinkmann, S. Faske, B. Koch, and M. Vogel, Z. Phys. Chem. **224**, 1535 (2010).

[11] M. Wilkening and P. Heitjans, Chem. Phys. Chem. **13**, 53 (2012).

[12] C. V. Chandran and P. Heitjans, Annu. Rep. NMR Spectrosc. **89**, 1 (2016).

[13] D. Brinkmann, Prog. Nucl. Magn. Reson. Spectrosc. **24**, 527 (1992).

[14] O. Kanert, R. Küchler, K. L. Ngai, and H. Jain, Phys. Rev. B **49**, 76 (1994).

[15] K. H. Kim, D. R. Torgeson, F. Borsa, J. Cho, S. W. Martin, and I. Svare, Solid State Ionics **91**, 7 (1996).

[16] R. Bertermann and W. Müller-Warmuth, Z. Naturforsch. **53a**, 863 (1998).

[17] J. Gabriel, O. V. Petrov, Y. Kim, S. W. Martin, and M. Vogel, Solid State Nucl. Magn. Reson. **70**, 53 (2015).

[18] M. Graf, B. Kresse, A. F. Privalov, and M. Vogel, Solid State Nucl. Magn. Reson. **51–52**, 25 (2013).

[19] K. Hayamizu and Y. Aihara, Solid State Ionics **238**, 7 (2013).

[20] Y. Onodera, K. Mori, T. Otomo, A. C. Hannon, S. Kohara, K. Itoh, M. Sugiyama, and T. Fukunaga, J. Phys. Soc. Jpn. **79**, 87 (2010).

[21] K. Mori, K. Enjuji, S. Murata, K. Shibata, Y. Kawakita, M. Yonemura, Y. Onodera, and T. Fukunaga, Phys. Rev. Appl. **4**, 054008 (2015).

[22] Y. Seino, M. Nakagawa, M. Senga, H. Higuchi, K. Takada, and T. Sasaki, J. Mater. Chem. A **3**, 2756 (2015).

[23] K. Hayamizu and Y. Aihara, Solid State Ionics **259**, 59 (2014).

[24] F. Fujara, D. Kruk, and A. F. Privalov, Prog. Nucl. Magn. Reson. Spectrosc. **82**, 39 (2014).

[25] B. Geil, Concepts Magn. Reson. **10**, 299 (1998).

[26] D. Kruk, A. Herrmann, and E. Rössler, Prog. Nucl. Magn. Reson. Spectrosc. **63**, 33 (2012).

[27] G. Balzer-Jöllenbeck, O. Kanert, H. Jain, and K. L. Ngai, Phys. Rev. B **39**, 6071 (1989).

[28] D. R. Figueroa, A. V. Chadwick, and J. H. Strange, J. Phys. C: Solid State Phys. **11**, 55 (1978).

[29] T. Klempt, O. Kanert, and D. Suter, Phys. Status Solidi B **236**, 151 (2003).

[30] E. Rössler, M. Taupitz, K. Börner, M. Schulz, and H.-M. Vieth, J. Chem. Phys. **92**, 5847 (1990).

[31] S. Faske, H. Eckert, and M. Vogel, Phys. Rev. B **77**, 104301 (2008).

[32] B. Koch and M. Vogel, Solid State Nucl. Magn. Reson. **34**, 37 (2008).

[33] M. Vogel, C. Brinkmann, H. Eckert, and A. Heuer, Phys. Chem. Chem. Phys. **4**, 3237 (2002).

[34] R. Richert and H. Bässler, J. Phys.: Condens. Matter **2**, 2273 (1990).